Solar cycle properties described by simple convection-driven dynamos

Radostin D Simitev[1,3] and **Friedrich H Busse**[2,3]

[1] School of Mathematics and Statistics, University of Glasgow – Glasgow G12 8QW, UK, EU
[2] Institute of Physics, University of Bayreuth – Bayreuth D-95440, Germany, EU
[3] NORDITA, AlbaNova University Center – Stockholm SE-10691, Sweden, EU

E-mail: busse@uni-bayreuth.de

Abstract

Simple models of magnetic field generation by convection in rotating spherical shells exhibit properties resembling those observed on the sun. The assumption of the Boussinesq approximation made in these models prevents a realistic description of the solar cycle, but through a physically motivated change in the boundary condition for the differential rotation the propagation of dynamo waves towards higher latitudes can be reversed at least at low latitudes.

Keywords: self-consistent MHD dynamos, solar dynamo

1. Introduction

A well known difficulty in modeling the solar dynamo is the fact that the dynamo waves which describe the nearly time periodic dynamics of the magnetic field tend to propagate from lower to higher latitudes instead in the opposite sense as observed on the sun. This effect is well known in mean field models of the solar cycle, see for example Stix (1976), but it is also observed in numerical solutions of convection-driven dynamos in rotating spherical fluid shells which are supposed to model processes in the solar convection zone. This shortcoming and others are caused by the inadequate representation of the compressibility of the solar atmosphere. Even with the huge power of modern supercomputers it is not yet possible to resolve adequately the dynamics of convection in the presence of the large density variation between bottom and top of the solar convection zone and to model appropriately the dependence of density on pressure.

In their early direct numerical models of solar convection and magnetic field generation, Gilman and Miller (1981) assumed the Boussinesq approximation in which the fluid is regarded as incompressible except in connection with the gravity term where the temperature dependence of the density is taken into account. This approximation eliminates the need for a separate equation of state and leads to a system of equations describing long period processes while the short period acoustic modes no longer enter the analysis. The same effect is obtained in the anelastic approximation in which the horizontally averaged density variation is taken into account, but the fluctuating component of the density is still only represented in the gravity term. For applications of the anelastic approximation in models of the solar convection zone see Gilman and Glatzmaier (1981) and Elliot et al. (2000).

Convection in rotating spherical fluid shells heated from below is always associated with a differential rotation generated by the Reynolds stresses of convection. An analytical model demonstrating the preference of banana shaped convection cells girdling the equator and the associated solar like differential rotation was presented by Busse (1970, 1973). While the analytical solution for stress-free boundaries exhibits a depth independent differential rotation, a differential rotation decreasing with depth is always found in fully nonlinear numerical models. This property together with the fact that the differential rotation reaches its maximum at the equator is responsible for the propagation of the dynamo waves towards higher latitudes (Yoshimura, 1975).

The solar differential rotation also decreases with depth throughout most of the convection zone with the exception of the tachocline region near its bottom and a region near its surface as indicated in figure 1(b). There is no general agreement about the origin of the upper 30Mm deep layer in which the differential rotation increases with depth. Here we assume that it is caused by supergranular convection that is characterized by a strong asymmetry between rising hot plasma and descending cool plasma. This type of convection has been modeled by hexagonal convection cells in the presence of rotation (Busse, 2007). As shown in this paper the asymmetry between rising and descending flow in hexagonal convection cells does indeed generate a differential rotation that increases with depth. We use this dynamical property of convection as motivation to modify the usually assumed stress-free boundary condition. Solely for

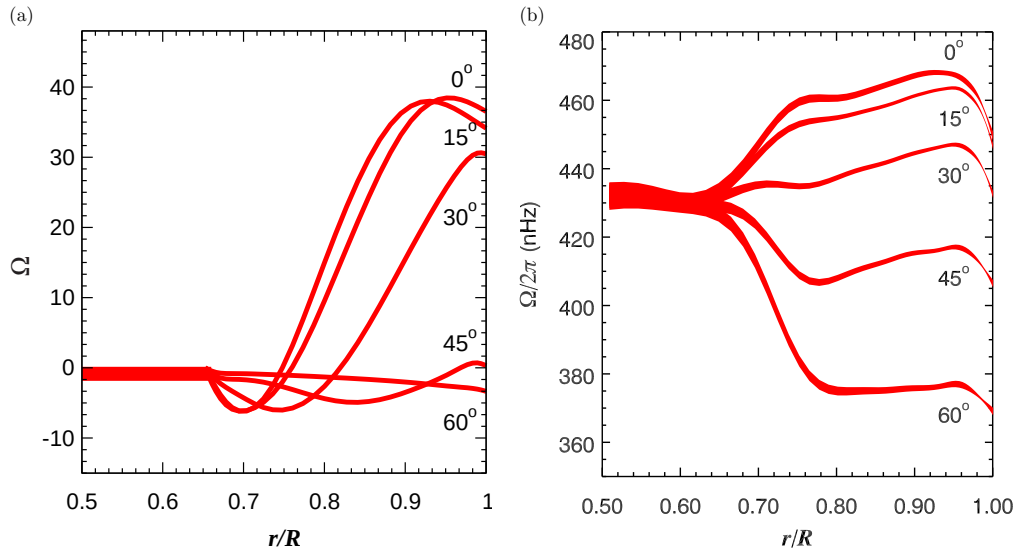

Figure 1: (color online) Differential rotation of the solar convection zone according to helioseismology (right, image courtesy NSF's National Solar Observatory) and differential rotation of the numerical model in the case $\eta = 0.65$, $P = 1$, $\tau = 2$, $R = 120000$, $P_m = 4$, $\beta = 1.5$ and mixed velocity boundary conditions (left).

the differential rotation we apply the condition given in expression (A11) of the Appendix. The resulting profiles shown in the example of figure 1(a) are still not very solar like, but they show an increase with depth of the differential rotation in the upper layer and tend to generate a more solar like behavior in the numerical simulations, as discussed below.

2. Simple Convection-Driven Dynamos

Because convection driven dynamo solutions strongly depend on the Prandtl number P and on the magnetic Prandtl number P_m for values of the order unity and because even bistability has been found in this parameter range (Simitev and Busse, 2009) we use a numerical model with a minimum number of external parameters as outlined in the Appendix. In this way it is possible to cover a relevant parameter region in sufficient detail. In addition to the two Prandtl numbers and the parameter β introduced in the boundary condition (A11), only the rotation parameter τ and the Rayleigh number R must be considered.

In choosing parameter values for a numerical solar model the task is most easily accomplished in the case of τ since only a value of the (eddy-) viscosity must be chosen. Using a commonly accepted eddy viscosity of the order $10^8 \mathrm{m}^2/\mathrm{s}$ (Gilman, 1983) we find $\tau \approx 2 \cdot 10^3$. It is more difficult to select an appropriate range for the Rayleigh number. We shall consider values that exceed the critical values for the onset of dynamo action by less than a factor of two. Otherwise convection motions become too chaotic and the structures of the dynamo solutions become less regular and more difficult to understand.

In figure 2 the properties of a convection-driven dynamo are indicated by following the nearly periodic magnetic field through half a magnetic cycle. The left column shows on the left side lines of constant magnetic flux density $\overline{B}_\varphi$ where the bar indicates the average over the azimuthal coordinate φ. On

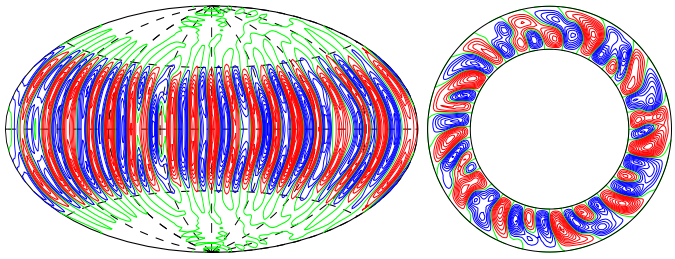

Figure 3: (color online) Contour lines of the radial velocity u_r at $r = r_i + 0.5$ and the poloidal streamlines $r\partial v/\partial\varphi$ in the equatorial plane in the case $P = 1$, $\tau = 2000$, $R = 120000$, $P_m = 4$, $\beta = 1.5$.

the right side of the meridional cross-section lines of the axisymmertic poloidal field are shown. The next column indicates the places where the toroidal field reaches its maximum strength near the surface. Since the toroidal field provides by far the major contribution to the horizontal magnetic flux density, eruptions of magnetic bipolar regions occur most likely at those places in the case of the sun. The modification of the stress-free boundary condition given by expression (A11) causes the differential rotation to increase with depth in the uppermost layer of the shell. This is turn causes the "magnetic bipolar regions" shown in the second column of figure 2 to drift in a solar-like fashion from higher latitudes towards the equator in agreement with solar observations. It is also remarkable that non-axisymmetric components characterized by the azimuthal wavenumber $m = 1$ of the magnetic field dominate over the axisymmetric component as is evident from the third column which shows the strength of the radial magnetic field at the surface of the sphere. The superposition of the axis- and non-axisymmetric components actually represent the property that the dynamo process is nearly confined to one meridional hemisphere while the other hemisphere is almost field free.

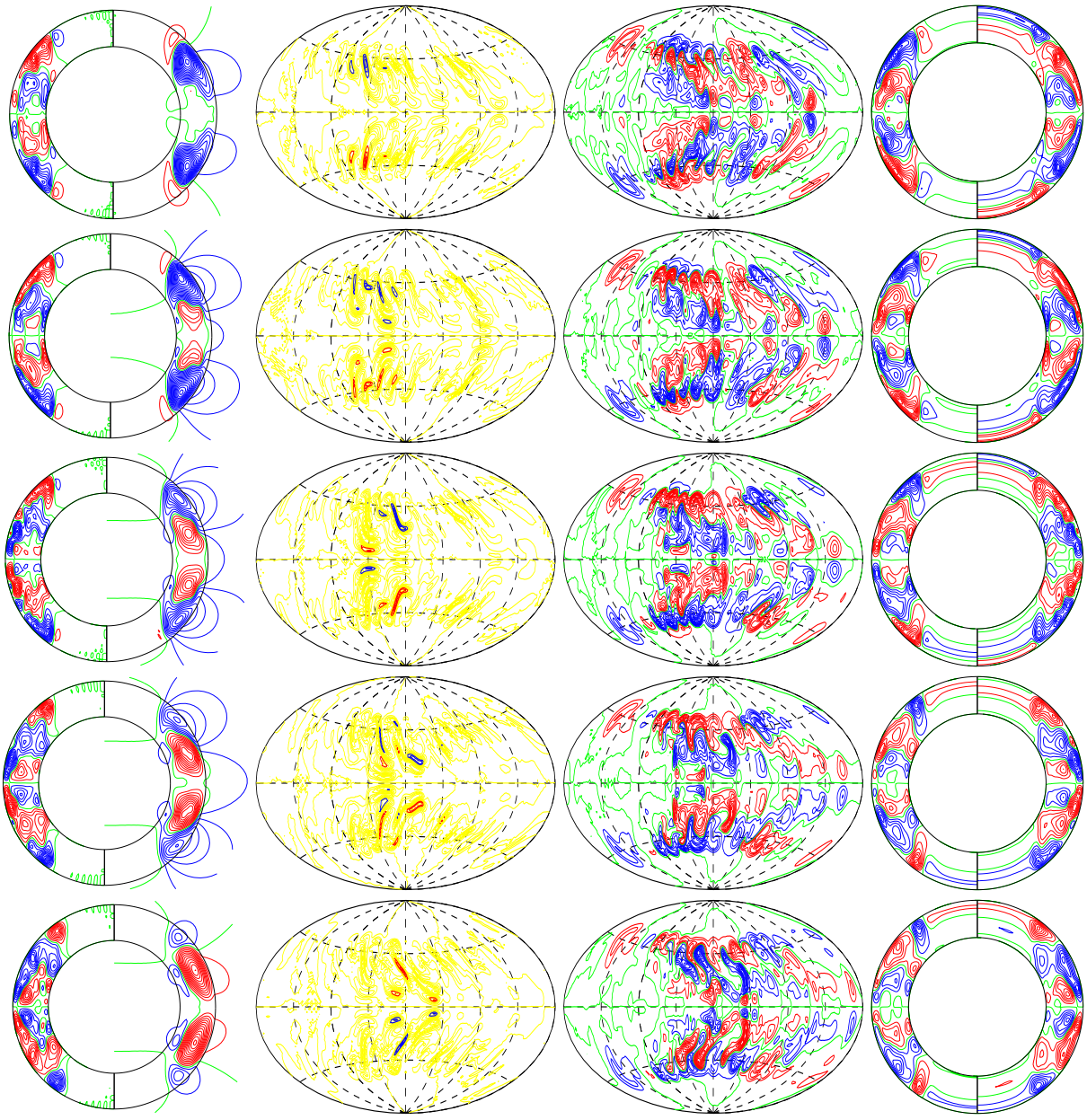

Figure 2: (color online)Approximately half a period of a dynamo oscillation in the case $\tau = 2000$, $R = 120000$, $P = 1$, $P_m = 4$, $\beta = 1.5$. The first column shows meridional lines of constant $\overline{B_\varphi}$ on the left and poloidal fieldlines, $r\sin\theta\partial\overline{h}/\partial\theta$ on the right. The second column shows lines of constant $\partial g/\partial\theta$ at $r = 0.9$ corresponding to -0.9, -0.8, -0.7, 0.7, 0.8, 0.9 of the maximum absolute value of $\partial g/\partial\theta$, and the third column shows lines of constant B_r at $r = r_o$. The last column shows Re($\partial g^{m=1}/\partial\theta$) on the left and Im($\partial g^{m=1}/\partial\theta$) on the right. The five rows are separated equidistantly in time by $\Delta t = 0.0224$.

The solar evidence for a non-axisymmetric magnetic field is provided by the phenomenon of active longitudes (see Usoskin et al. (2007) and references therein). As in the case of those longitudes, the field shown in the third column of figure 2 hardly propagates throughout the time frame of the figure. The angular velocity of the prograde propagation of the pattern is less than 2π which is similar to the propagation of the convection pattern. In contrast to the cyclical nature of the magnetic field the convection pattern is nearly steady as indicated in figure 3. Individual convection columns may sometimes breakup in that the outer part tends to propagate a bit faster than the inner part which essentially remains steady in the rotating frame.

In figure 4 half a magnetic cycle is presented for a higher Rayleigh number than in the case of figure 2. As is evident from the 3 column of figure 4 the structure of the magnetic field is not antisymmetric with respect to the equatorial plane. In the southern hemisphere the $m = 2$ –component of the magnetic field dominates in this particular cycle. At other times patterns that are more antisymmetric and similar to that shown in figure 2 are found. The amplitude of the magnetic field varies strongly from cycle to cycle as shown in figure 5 while amplitude of convection exhibits rather small variations.

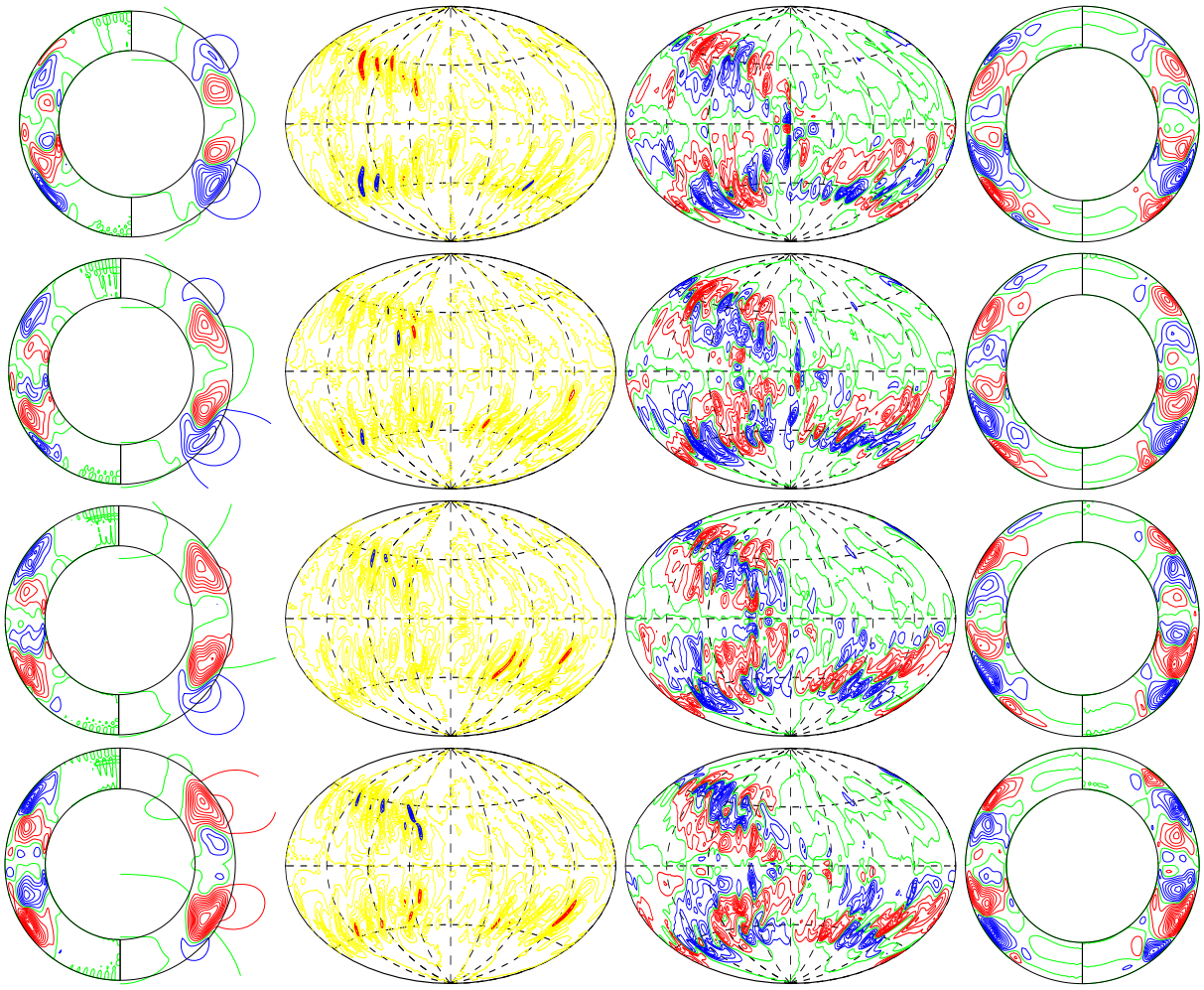

Figure 4: (color online)Nearly half a period of a dynamo oscillation in the case $\tau = 2000$, $R = 140000$, $P = 1$, $P_m = 3.5$, $\beta = 1.0$. The first column shows meridional lines of constant $\overline{B_\varphi}$ on the left and poloidal fieldlines, $r\sin\theta\partial\overline{h}/\partial\theta$ on the right. The second column shows contour lines of $|B_{horizontal}|\mathrm{sgn}(B_\varphi)$ at $r = 0.9$ corresponding to -0.9, -0.8, -0.7, 0.7, 0.8, 0.9 of the maximum value of $|B_{horizontal}|$, and the third column shows lines of constant B_r at $r = r_o$. The last column shows $\mathrm{Re}(\partial g^{m=2}/\partial\theta)$ on the left and $\mathrm{Im}(\partial g^{m=2}/\partial\theta)$ on the right. The four rows are separated equidistantly in time by $\Delta t = 0.0168$.

It is tempting to present visualizations similar to the famous butterfly diagrams of solar cycles that have recorded observations of sunspots for many decades. Since we associate the occurrence of sunspots with the strength of the horizontal component of the magnetic field in the sun near the surface, the amplitudes of the maximum values of the horizontal components could be plotted as function of latitude and time. But this procedure could not be realized due to limitations of data storage. Instead we have restricted the attention to the main contributer to the azimuthal component of the magnetic field. Thus, in the top panel of figure 6 the extremal azimuthal component of the magnetic field corresponding to the wave numbers $m = 0$ and $m = 1$, i.e. $\overline{B_\varphi}+|B_\varphi^{m=1}|\mathrm{sgn}(\overline{B_\varphi})$, is plotted as function of time and latitude. In contrast to solar butterfly diagrams the movements to higher latitudes still dominate over the movements towards lower latitudes. The latter are only visible in the form of streaks at lower latitudes. For comparison the same quantity, but with $m = 1$ replaced by $m = 2$, has been plotted in bottom panel of figure 6. The similarity between the two plots indicates that the time and latitude dependence of the extremal values of B_φ can approximately be captured in this way.

In addition to butterfly diagrams based on sunspots also butterfly diagrams based on observations of the radial component of the magnetic field are often used. In the middle panel of figure 6 a theoretical butterfly diagram is shown where $\overline{B_r}+|B_r^{m=1}|\mathrm{sgn}(\overline{B_r})$ has been plotted as function of time and latitude. A comparison of the top and the middle panels of figure 6 indicates a noticeable phase shift between the two diagrams which agrees roughly with the well known observation that the radial component of the solar magnetic field changes its sign near the maximum of the solar cycle (Stix, 1976).

3. Conclusion

In this report an attempt is described to explore the extent to which the operation of the solar dynamo can be understood on the basis of a minimal, but physically consistent, convection-driven dynamo model. Although the Boussinesq approxima-

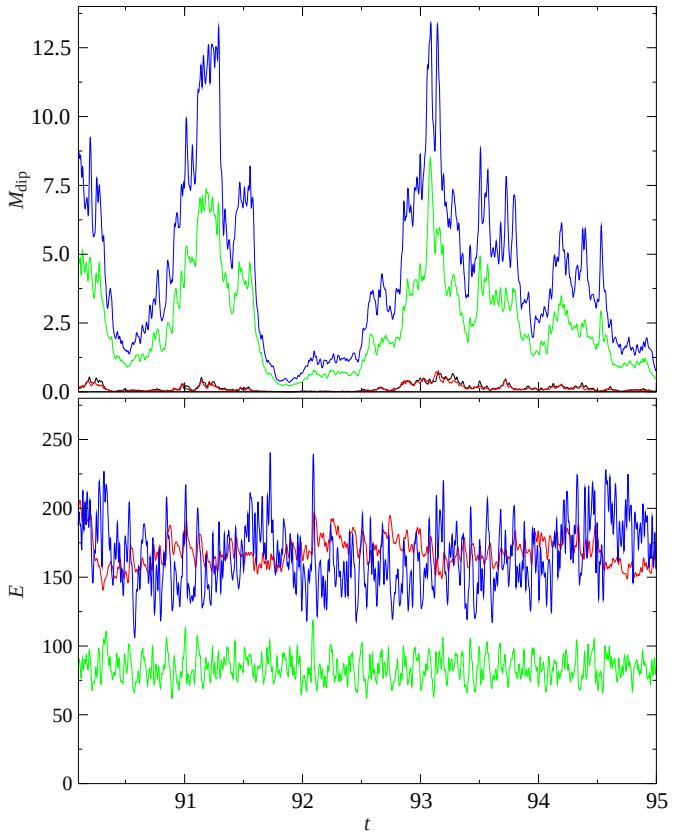

Figure 5: (color online) Time series of magnetic dipolar energy densities and kinetic energy densities in the upper and lower panel respectively. The component $\overline{X}_p$ is shown by solid black line, while $\overline{X}_t$, $\check{X}_p$, and $\check{X}_t$ are shown by red, green and blue lines, respectively. X stands for either $M_{\rm dip}$ or E. The parameter values are $P = 1$, $\tau = 2000$, $R = 140000$, $P_m = 3.5$, $\beta = 1$.

tion is a highly unrealistic assumption in the case of the Sun, the convection columns are similar to those found in numerical simulations based on anelastic models, see, for instance, Brun et al. (2004) and Ghizaru et al. (2010). Although there is little solar evidence for this type of convection, there are generally believed to exist as "giant cells" in the deeper region of the solar convection zone.

The structure of the magnetic field found in our simulations differs substantially from the commonly assumed structure of the solar magnetic field dominated by a strong axisymmetric toroidal component. When the evidence for this traditional view is examined, however, it is found that observations do not contradict fields dominated by $m = 1$ or $m = 2$ components such as those shown in figures 2 and 5. On the contrary, the presence of active longitudes on the sun indicates at least that components with the azimuthal wavenumbers $m = 1$ and $m = 2$ play a significant role.

A more detailed exploration of the parameter space of our minimal model is likely to reveal an even better correspondence with solar observations.

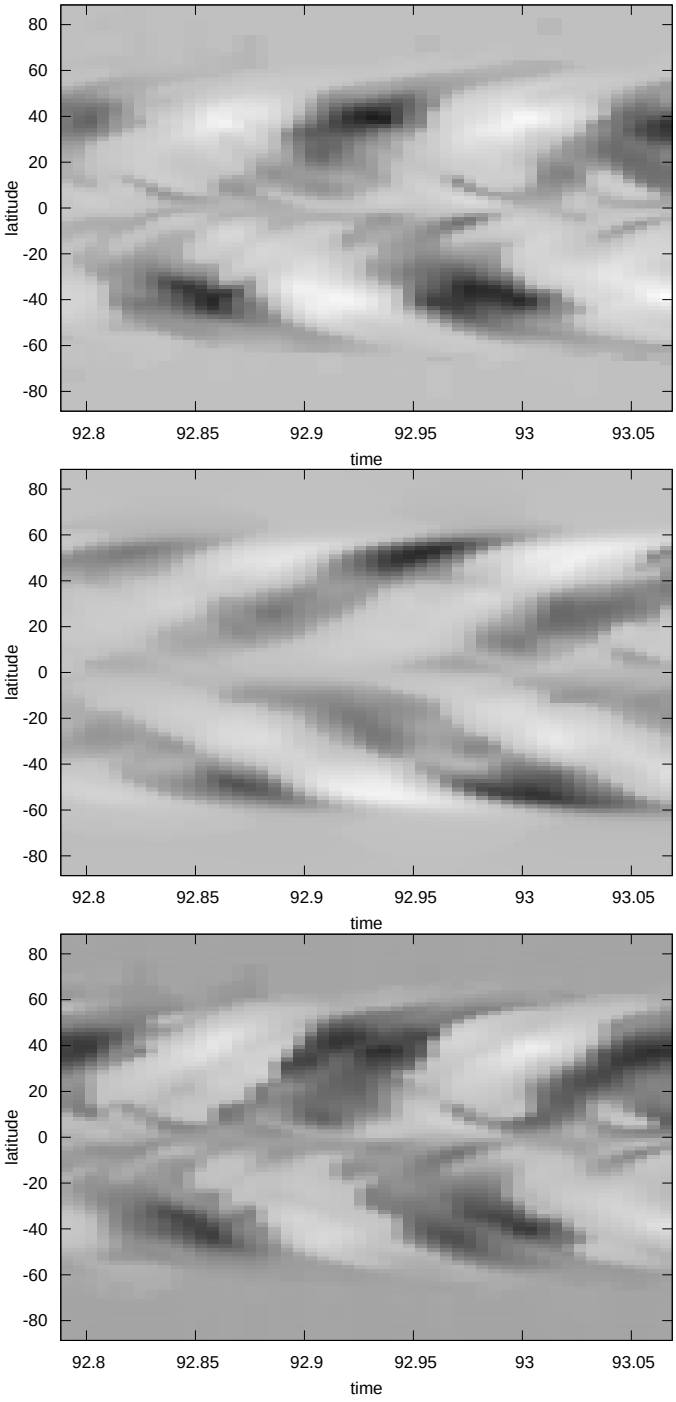

Figure 6: "Butterfly" diagrams: $B_\varphi^{m=0} + |B_\varphi^{m=1}|\mathrm{sgn}(B_\varphi^{m=0})$ (top), $B_r^{m=0} + |B_r^{m=1}|\mathrm{sgn}(B_r^{m=0})$ (middle), and $B_\varphi^{m=0} + |B_\varphi^{m=2}|\mathrm{sgn}(B_\varphi^{m=0})$ (bottom) are plotted as functions of latitude and time in the case $P = 1$, $\tau = 2000$, $R = 140000$, $P_m = 3.5$, $\beta = 1$.

Appendix A. Mathematical Formulation of the Numerical Model

In the numerical model a spherical fluid shell rotating about a fixed axis described by the unit vector $\boldsymbol{k}$ is considered. It is assumed that a static state exists with the temperature distribu-

tion

$$T_S = T_0 + \Delta T \eta r^{-1}(1-\eta)^{-2},$$

where r denotes the distance from the center of the spherical shell measured in terms of multiples of the shell thickness d and η denotes the ratio of inner to outer radius of the shell. ΔT is the temperature difference between the two boundaries. The gravity field is given by $\boldsymbol{g} = -d\gamma\boldsymbol{r}$. In addition to d, the time d^2/ν, the temperature $\nu^2/\gamma\alpha d^4$, and the magnetic flux density $\nu(\mu\varrho)^{1/2}/d$ are used as scales for the dimensionless description of the problem where ν denotes the kinematic viscosity of the fluid, κ its thermal diffusivity, ϱ its density and μ is its magnetic permeability. The equations of motion for the velocity vector $\boldsymbol{u}$, the heat equation for the deviation Θ from the static temperature distribution, and the equation of induction for the magnetic flux density $\boldsymbol{B}$ are thus given by

$$\partial_t \boldsymbol{u} + \boldsymbol{u}\cdot\nabla\boldsymbol{u} + \tau\boldsymbol{k}\times\boldsymbol{u} = -\nabla\pi + \Theta\boldsymbol{r} + \nabla^2\boldsymbol{u} + \boldsymbol{B}\cdot\nabla\boldsymbol{B}, \quad \text{(A.1)}$$

$$\nabla\cdot\boldsymbol{u} = 0, \quad \text{(A.2)}$$

$$P(\partial_t\Theta + \boldsymbol{u}\cdot\nabla\Theta) = (R\eta r^{-3}(1-\eta)^{-2})\boldsymbol{r}\cdot\boldsymbol{u} + \nabla^2\Theta, \quad \text{(A.3)}$$

$$\nabla\cdot\boldsymbol{B} = 0, \quad \text{(A.4)}$$

$$\nabla^2\boldsymbol{B} = P_m(\partial_t\boldsymbol{B} + \boldsymbol{u}\cdot\nabla\boldsymbol{B} - \boldsymbol{B}\cdot\nabla\boldsymbol{u}), \quad \text{(A.5)}$$

where ∂_t denotes the partial derivative with respect to time t and where all terms in the equation of motion that can be written as gradients have been combined into $\nabla\pi$. The Boussinesq approximation is assumed in that the density ϱ is regarded as constant except in the gravity term where its temperature dependence, given by $\alpha \equiv -(\partial\varrho/\partial T)/\varrho = const.$, is taken into account. The Rayleigh numbers R, the Coriolis number τ, the Prandtl number P and the magnetic Prandtl number P_m are defined by

$$R = \frac{\alpha\gamma\Delta T d^4}{\nu\kappa}, \quad \tau = \frac{2\Omega d^2}{\nu}, \quad P = \frac{\nu}{\kappa}, \quad P_m = \frac{\nu}{\lambda}, \quad \text{(A.6)}$$

where λ is the magnetic diffusivity. Because the velocity field $\boldsymbol{u}$ as well as the magnetic flux density $\boldsymbol{B}$ are solenoidal vector fields, the general representation in terms of poloidal and toroidal components can be used,

$$\boldsymbol{u} = \nabla\times(\nabla v\times\boldsymbol{r}) + \nabla w\times\boldsymbol{r}\ , \quad \text{(A.7)}$$

$$\boldsymbol{B} = \nabla\times(\nabla h\times\boldsymbol{r}) + \nabla g\times\boldsymbol{r}\ . \quad \text{(A.8)}$$

Equations for v and w are obtained by multiplication of the curl[2] and of the curl of equation (1) by $\boldsymbol{r}$. Analogously equations for h and g are obtained through the multiplication of equation (4) and of its curl by $\boldsymbol{r}$.

No-slip boundary conditions are used at the inner boundary and stress-free conditions are applied at the outer boundary, while the temperature is assumed to be fixed at both boundaries,

$$v = \partial_r v = w = \Theta = 0 \quad \text{at } r = r_i \equiv \eta/(1-\eta) \quad \text{(A.9)}$$

$$v = \partial_{rr}^2 v = \partial_r(w/r) = \Theta = 0 \quad \text{at } r = r_o \equiv 1/(1-\eta). \quad \text{(A.10)}$$

Only the value $\eta = 0.65$ is used in the present paper. An exception from the stress-free boundary at $r = r_o$ will be assumed for the axisymmetric part $\overline{w}$ of w,

$$\partial_r(\overline{w}/r) = -\beta\overline{w}/r. \quad \text{(A.11)}$$

For the magnetic field, electrically insulating boundaries are assumed such that the poloidal function h must be matched to the function $h^{(e)}$, which describes the potential fields outside the fluid shell

$$g = h - h^{(e)} = \partial_r(h - h^{(e)}) = 0 \text{ at } r = r_i \text{ and at } r = r_o. \quad \text{(A.12)}$$

The numerical integration proceeds with the pseudo-spectral method as described by Tilgner (1999) which is based on an expansion of all dependent variables in spherical harmonics for the θ,φ-dependences, i.e.

$$v = \sum_{l,m} V_l^m(r,t)P_l^m(\cos\theta)\exp(im\varphi) \quad \text{(A.13)}$$

and analogous expressions for the other variables, w, Θ, h and g. Here P_l^m denotes the associated Legendre functions. For the r-dependence expansions in Chebychev polynomials are used. For the computations to be reported in this paper a minimum of 41 collocation points in the radial direction and spherical harmonics up to the order 128 have been used.

The magnetic energy density components of dynamo solutions are defined as

$$\overline{M}_p = \frac{1}{2}\langle|\ \nabla\times(\nabla\overline{h}\times\boldsymbol{r})\ |^2\rangle, \quad \overline{M}_t = \frac{1}{2}\langle|\ \nabla\overline{g}\times\boldsymbol{r}\ |^2\rangle,$$

$$\check{M}_p = \frac{1}{2}\langle|\ \nabla\times(\nabla\check{h}\times\boldsymbol{r})\ |^2\rangle, \quad \check{M}_t = \frac{1}{2}\langle|\ \nabla\check{g}\times\boldsymbol{r}\ |^2\rangle,$$

where $\langle\cdot\rangle$ indicates the average over the fluid shell and $\overline{h}$ refers to the axisymmetric component of h, while $\check{h}$ is defined by $\check{h} = h - \overline{h}$. The corresponding kinetic energy densities $\overline{E}_p$, $\overline{E}_t$, $\check{E}_p$ and $\check{E}_t$ are defined analogously with v and w replacing h and g.

Acknowledgement

The research reported in this paper was performed in parts during the authors' participation in the 2011 program "Dynamo, Dynamical Systems and Topology" at NORDITA. The research of R.S. has also been supported by the UK Royal Society under Research Grant 2010 R2. The research of F.B. has also been supported by NASA Grant NNX09AJ85G. The authors are indebted to Prof. A. Kosovichev for his continuing encouragement.

References

Brun, A. S., Miesch, M. S., and Toomre, J., 2004, Astrophys. J., 614, 1073
Busse, F. H., 1970, Astrophys. J., 159, 629
Busse, F. H., 1973, Astron. Astrophys., 28, 27
Busse, F. H., 2007, Sol. Phys. 245, 27
Ghizaru, M., Charbonneau, P., & Smolarkiewicz, P. K., 2010, Astrophys. J. Lett. 715, L133-L137
Gilman, P. A., 1983, Astrophys. J. Suppl., 53, 243
Gilman, P. A., & Glatzmaier, G. A., 1981, Astrophys. J. Suppl., 45, 335
Elliott, J. R., Miesch, M. S., & Toomre, J., 2000, Astrophys. J., 533, 546
Simitev R., and Busse F. H., 2010, EPL, 85, 19001
Stix, M., 1976, in IAU Symposium 71, Basic Mechanism of Solar Activity, ed. V. Bumba & J. Kleczek (Dordrecht: Reidel), p.367
Stix, M., 1976, Astron. Astrophys., 47, 243-254
Tilgner A., 1999, Int. J. Num. Meth. Fluids, 30, 713
Usoskin, I. G., Berdyugina, S. V., Moss, D., & Sokoloff, D. D., 2007, Adv. Space Res. 40, 951-958
Yoshimura, H., 1975, Astrophys. J., 201, 740